This is the Author Accepter Manuscript (AAM). The published version is available online since 9 June, 2022 at https://dx.doi.org/10.1016/j.camwa.2022.05.023 under subscription to Elsevier B.V.:
Computers & Mathematics with Applications Volume 119, 1 August 2022, Pages 1-12

# Bend 3d Mixed Virtual Element Method for Darcy problems

Franco Dassi[a], Alessio Fumagalli[b,*], Anna Scotti[b], Giuseppe Vacca[c]

[a] *Dipartimento di Matematica e Applicazioni, Università degli Studi di Milano Bicocca, Via Roberto Cozzi 55 - 20125 Milano, Italy*
[b] *MOX - Dipartimento di Matematica "F. Brioschi", Politecnico di Milano, via Bonardi 9, 20133 Milan, Italy*
[c] *Dipartimento di Matematica, Università di Bari, via E. Orabona 4, 70125 Bari, Italy*

**Abstract**

In this study, we propose a virtual element scheme to solve the Darcy problem in three physical dimensions. The main novelty is that curved elements are naturally handled without any degradation of the solution accuracy. Indeed, in presence of curved boundaries, or internal interfaces, the geometrical error introduced by planar approximations may dominate the convergence rate limiting the benefit of high-order approximations. We consider the Darcy problem in its mixed form to directly obtain accurate and mass conservative fluxes without any post-processing. An important step to derive the proposed scheme is the integration over curved polyhedrons, here presented and discussed. Finally, we show the theoretical analysis of the scheme as well as several numerical examples to support our findings.

*Keywords:* Mixed VEM, Curved faces, High order approximations, Integration over curved polyhedrons

## 1. Introduction

Fluid flow in porous media is a broad research area that involves scientists as well as engineers from both private and public sector due to its relevance in energy management, for instance hydrocarbon extraction, long term $CO_2$ sequestration, geothermal extraction and storage, as well as in several applications in industry and life science. Moreover, an interesting and current application is the prevention of groundwater pollution due to human activities like landfills leakage, nuclear waste disposal, and remediation of polluted industrial sites, see e.g. [1, 2].

*Corresponding author
*Email addresses:* franco.dassi@unimib.it (Franco Dassi), alessio.fumagalli@polimi.it (Alessio Fumagalli ), anna.scotti@polimi.it (Anna Scotti), giuseppe.vacca@uniba.it (Giuseppe Vacca)

In subsurface flow simulations, and in particular in oil field modeling, non standard grids are often employed to honor the domain geometry. One example are the so-called corner-point grids which are composed by hexahedrons whose facets are curved, more specifically they are bilinear functions [3]. To compute geometrical properties on such meshes, the standard approach consists in discretizing these cells by means of suitable sub-grids. However, in the presence of particular configurations, such as pinched or highly distorted elements, the geometrical error introduced by this approximation based on a sub-tetrahedrization, may pollute the accuracy of the whole solution. In the context of the Finite Element Method (FEM), an accurate description of the curved geometry is a key point to preserve the quality of the solution itself especially for high order approximations.

In this paper, we propose a new numerical strategy to overcome this issue, i.e., we propose a method that avoids any geometrical error and incorporates the presence of cells with curved faces without the need for sub-tetrahedrization. Such strategy is based on the Virtual Element Method (VEM) which can be seen as an extension of the FEM to deal with polygonal/polyhedral grids. Indeed, it follows mostly the classical finite element framework but the key point is that the basis functions are left unknown and never explicitly computed [4]. It was successfully exploited for the numerical solution of both 2d and 3d problems see, e.g., [5, 6, 7, 8, 9, 10]. The possibility to deal with elements characterized by very general shape (also non-covex) is appealing for real life problems. Other strategies, that are able to handle curved geometries, include Discontinuous Galerkin [11, 12, 13, 14] approximations as well as Hybrid High Order schemes [15].

The possibility to handle elements with curved edges in the VEM framework has been introduced in the seminal works [16, 17, 18] for the two-dimensional case. Moreover, the authors in [19] modified the virtual element space of [16] to contain polynomials, since we will see that this is not true a-priori. This step is crucial to preserve the expected convergence rates in the degenerate case of an element with decreasing diameter while keeping boundary curvature fixed.

In this paper we are modelling a single-phase flow in porous media via a mixed formulation, i.e., we consider both the macroscopic (or Darcy) velocity and the pressure as unknowns. Although we have to solve a linear system with a saddle-point structure, such formulation has several advantages. Indeed, it gives a velocity field that is locally mass conservative and thus perfectly suited for the subsequent simulation of other processes, such as transport phenomena. It is also suited for applications with strong variations in the coefficients, typically permeability, see, e.g., [20, 21, 22, 23, 24] and [25, 6, 26, 27, 28, 29] in the context of FEM and VEM, respectively. In particular VEM have already been extensively employed in reservoir simulations, where meshes are characterized by involved geometries due to the presence of fractures and faults, see for instance [30, 27, 31, 28, 29, 32]. Finally, in the recent works [33] VEM has been successfully applied to $p$ and $hp$ adaptivity and the coupling between VEM and the Boundary Element Method (BEM) in [34].

The main contribution of this work is to introduce, analyze and validate the Mixed Virtual Element Method (MVEM) for problems characterized by curved

boundaries or internal curved interfaces in three dimensions. The piece-wise planar approximation of these surfaces, which is often used in practice with traditional methods, introduces a geometrical error that corrupts the optimal error decay, especially in the high order case. To obtain a high order approximation with curved geometries, we proceed on two fronts. On one hand we extend the quadrature rules for curved polygons introduced in [35, 36, 16] to deal with polyhedrons characterized by curved faces. On the other hand we define the MVEM spaces for curved geometries in three dimensions and prove the main properties of the method. The method can be regarded as an extension of what has been proposed in [17] for the 2d case, but presents new challenges at the technical level.

This paper is organized as follows. In Section 2 we introduce some notation useful for the rest of the work, we present the mathematical problem in its strong and weak formulation and we detail the assumptions on the domain. Section 3 contains the detailed description of the MVEM spaces and the construction of the approximated forms. In Section 4 we provide the interpolation error analysis for the virtual element space, the velocity space. In Section 5 we describe the quadrature rules exploited to integrate function in polyhedrons characterized by curved faces. In Section 6 some numerical academic tests are performed to validate the proposed approach. Furthermore, the proposed method is also applied to a numerical experiment inspired from real life applications characterized by the presence of corner point cells. Finally, in Section 7, we draw some conclusions.

## 2. Notations and preliminaries

In the present section we introduce some basic tools and notations useful in the construction and theoretical analysis of VEM.

### *2.1. Functional spaces*

Throughout the paper, we will follow the usual notation for Sobolev spaces and norms [37]. Hence, for an open bounded domain $\omega$, the norms in the spaces $W_p^s(\omega)$ and $L^p(\omega)$ are denoted by $\|\cdot\|_{W_p^s(\omega)}$ and $\|\cdot\|_{L^p(\omega)}$, respectively. Norm and seminorm in $H^s(\omega)$ are denoted respectively by $\|\cdot\|_{s,\omega}$ and $|\cdot|_{s,\omega}$, while $(\cdot,\cdot)_\omega$ and $\|\cdot\|_\omega$ denote the $L^2$-inner product and the $L^2$-norm (the subscript $\omega$ may be omitted when $\omega$ is the whole computational domain $\Omega$). To keep the notation simpler, we adopt the notations above also for the vector and tensor valued functional spaces $[W_p^s(\omega)]^{d_1\times d_2}$ with $d_1,\, d_2 \geq 1$.

Here below we fix some additional notation of the multivariable calculus in 3d. We denote with $\boldsymbol{x} = (x_1,\, x_2,\, x_3)$ the independent variable. With a usual notation the symbols $\nabla$ and $\Delta$ denote the gradient and Laplacian for scalar functions, while $\boldsymbol{\Delta}$, $\boldsymbol{\nabla}$, div and **curl** denote the vector Laplacian, the gradient, the divergence and the curl operator for vector fields. Letting $\omega \subset \mathbb{R}^3$ we recall

the following well-known functional spaces:

$$H(\mathrm{div},\omega) := \{\boldsymbol{v} \in [L^2(\omega)]^3 : \mathrm{div}\,\boldsymbol{v} \in L^2(\omega)\},$$
$$H(\mathbf{curl},\omega) := \{\boldsymbol{v} \in [L^2(\omega)]^3 : \mathbf{curl}\,\boldsymbol{v} \in [L^2(\omega)]^3\},$$

with scalar products and induced norms indicated as $(\cdot,\cdot)_{H(\mathrm{div},\omega)}$ and $\|\cdot\|_{H(\mathrm{div},\omega)}$, and $(\cdot,\cdot)_{H(\mathbf{curl},\omega)}$ and $\|\cdot\|_{H(\mathbf{curl},\omega)}$, respectively. Let $\gamma \subset \partial\omega$ and let $\boldsymbol{n}$ be the unit exterior normal vector to $\gamma$, we introduce the following subspaces of $H(\mathrm{div},\omega)$ and $H(\mathbf{curl},\omega)$:

$$H_\gamma(\mathrm{div},\omega) := \{\boldsymbol{v} \in H(\mathrm{div},\omega) : \boldsymbol{v}\cdot\boldsymbol{n} = 0 \text{ on } \gamma\},$$
$$H_\gamma(\mathbf{curl},\omega) := \{\boldsymbol{v} \in H(\mathbf{curl},\omega) : \boldsymbol{v}\wedge\boldsymbol{n} = \boldsymbol{0} \text{ on } \gamma\},$$

where, we indicate with $\wedge$ the cross product between two vectors.

*2.2. Model Problem*

In the present subsection, we introduce the mathematical model we are interested to solve. We consider a three-dimensional domain $\Omega \subset \mathbb{R}^3$, whose boundary $\partial\Omega$ is Lipschitz continuous with unit normal $\boldsymbol{n}$ pointing outward from $\Omega$. We stress the fact that the boundary, or a portion of it, might be curved (see also Subsection 2.3). To impose suitable boundary conditions, we divide $\partial\Omega$ into two distinct parts: $\partial_e\Omega$ and $\partial_n\Omega$. In the former we set essential boundary conditions and in the latter natural ones. We clearly have $\overline{\partial\Omega} = \overline{\partial_e\Omega}\cup\overline{\partial_n\Omega}$ and $\partial_e^\circ\Omega \cap \partial_n^\circ\Omega = \emptyset$. Finally, for solvability issues we assume that $\partial_n^\circ\Omega \neq \emptyset$.

The domain $\Omega$ represents a porous medium saturated by a single fluid (e.g., water). The porous medium is characterized by $\kappa$, the permeability tensor, assumed to be symmetric and positive defined, while the fluid is characterized by a dynamic viscosity $\mu$ which is a strictly positive number. External forces are the vector $\boldsymbol{g}$ and scalar $\varsigma$ sources; $\boldsymbol{g}$ might represent a gravity term and $\varsigma$ the effect of an injection or extraction well. On $\partial\Omega$ boundary conditions on the pressure $\overline{p}$ or on the normal flux $\overline{q}$ might be imposed.

Since we are considering a Darcy problem in mixed form the unknowns are the Darcy velocity $\boldsymbol{q}$ and the fluid pressure $p$, which are solution of the following problem.

**Problem 1 (Darcy problem - strong form).** *Find* $(\boldsymbol{q}, p)$ *such that*

$$\begin{cases} \mu\boldsymbol{q} + \kappa\nabla p = \boldsymbol{g} \\ \mathrm{div}\,\boldsymbol{q} = \varsigma \end{cases} \quad \text{in } \Omega \qquad \begin{cases} p = \overline{p} & \text{on } \partial_n\Omega \\ \boldsymbol{q}\cdot\boldsymbol{n} = \overline{q} & \text{on } \partial_e\Omega \end{cases}$$

To derive the weak form of Problem 1, we introduce the following functional spaces for vector and scalar fields

$$\boldsymbol{V} := H_{\partial_e\Omega}(\mathrm{div},\Omega) \quad \text{and} \quad Q := L^2(\Omega).$$

We indicate the scalar products and induced norms of these spaces as: $(\cdot,\cdot)_{\boldsymbol{V}}$ and $\|\cdot\|_{\boldsymbol{V}}$, and $(\cdot,\cdot)_Q$ and $\|\cdot\|_Q$ respectively. By setting $\lambda = \mu\kappa^{-1}$, we introduce the following forms

$$\begin{aligned} &a : \boldsymbol{V} \times \boldsymbol{V} \to \mathbb{R} \quad a(\boldsymbol{u},\boldsymbol{v}) := (\lambda\boldsymbol{u},\boldsymbol{v})_\Omega && \forall (\boldsymbol{u},\boldsymbol{v}) \in \boldsymbol{V}\times\boldsymbol{V}\,, \\ &b : \boldsymbol{V} \times Q \to \mathbb{R} \quad b(\boldsymbol{u},v) := -(\operatorname{div}\boldsymbol{u},v)_\Omega && \forall (\boldsymbol{u},v) \in \boldsymbol{V}\times Q\,. \end{aligned} \tag{1}$$

Moreover, we introduce the functionals

$$\begin{aligned} &G : \boldsymbol{V} \to \mathbb{R} \quad G(\boldsymbol{v}) := -(\overline{p},\boldsymbol{v}\cdot\boldsymbol{n})_{\partial_n\Omega} + (\kappa^{-1}\boldsymbol{g},\boldsymbol{v})_\Omega && \forall \boldsymbol{v} \in \boldsymbol{V}\,, \\ &F : Q \to \mathbb{R} \quad F(v) := -(\varsigma,v)_\Omega && \forall v \in Q\,. \end{aligned} \tag{2}$$

For the data, we assume the following regularity conditions: $\kappa \in [L^\infty(\Omega)]^{3\times 3}$, $\mu \in L^2(\Omega)$, $\overline{p} \in H^{\frac{1}{2}}_{00}(\partial_n\Omega)$, $\boldsymbol{g} \in [L^2(\Omega)]^3$, and $\varsigma \in L^2(\Omega)$. With this in place, we can introduce the weak form of Problem 1 by assuming $\overline{q} = 0$.

**Problem 2 (Darcy problem - weak form).** *Find $(\boldsymbol{q},p) \in \boldsymbol{V}\times Q$ such that*

$$\begin{cases} a(\boldsymbol{q},\boldsymbol{v}) + b(\boldsymbol{v},p) = G(\boldsymbol{v}) & \forall \boldsymbol{v} \in \boldsymbol{V}\,, \\ b(\boldsymbol{q},v) = F(v) & \forall v \in Q\,. \end{cases}$$

Following, e.g., [24] it is possible to show that Problem 2 is well-posed.

**Remark 1.** *We have used an abuse in notation for the term $(\overline{p},\boldsymbol{v}\cdot\boldsymbol{n})_{\partial_n\Omega}$, in fact the first entry is an element of $H^{\frac{1}{2}}_{00}(\partial_n\Omega)$ and the second of $H^{-\frac{1}{2}}(\partial_n\Omega)$, being the latter a trace of a $H(\operatorname{div},\Omega)$ function. To be precise, we should use a duality pairing between them and write $\langle \overline{p},\boldsymbol{v}\cdot\boldsymbol{n}\rangle_{H^{\frac{1}{2}}_{00}(\partial_n\Omega)\times H^{-\frac{1}{2}}(\partial_n\Omega)}$ in place of the $L^2$-scalar product.*

*2.3. Assumption on the curved domains*

In the following we detail the assumption on the (curved) domain $\Omega$. Extending to the 3d case the approach in [16, 17], we consider a bounded Lipschitz domain $\Omega$ whose boundary $\partial\Omega$ is made up of a finite number of smooth surfaces $\{\Gamma_i\}_{i=1,\dots,N}$ that fit the boundary, split into "essential" and "natural" part, i.e.,

$$\cup_{i=1}^{N_e}\Gamma_i = \partial_e\Omega \qquad \text{and} \qquad \cup_{i=N_e+1}^{N}\Gamma_i = \partial_n\Omega.$$

We assume that:

**Assumption 1 (Boundary regularity).** *Each surface $\Gamma_i$ is a regular surface and there exists a sufficiently regular and invertible function $\gamma_i\colon \mathfrak{F}_i \to \Gamma_i$ where $\mathfrak{F}_i \subset \mathbb{R}^2$.*

Since all the parts $\Gamma_i$ of $\partial\Omega$ will be treated in the same way, in the following we will drop the index $i$ from all the involved maps and parameters to obtain a lighter notation.

**Remark 2 (Internal interfaces).** *It is important to note that proposed approach is also valid for internal curved interfaces. However, to keep the presentation simpler we assume only curved elements on the boundary, being its extension straightforward. The example in Subsection 6.3 deals with internal interfaces.*

## 3. Mixed Virtual Elements on curved polyhedra

In the present section, we define the virtual formulation of Problem 2. We first discuss the assumptions for meshes on the curved domain $\Omega$, then we introduce the space for vector and scalar fields with the associated sets of degrees of freedom. To discretize Problem 2, when the computational domain presents curved boundaries or interfaces, we extend the discrete spaces proposed in [25] via the idea proposed in [16]. In Subsection 3.1 we detail the mesh assumptions, in Subsection 3.2 we fix some notations for polynomials and we introduce the polynomial projections. In Subsection 3.3 we describe the virtual element velocities spaces and the associated pressures space. In Subsections 3.4 we present the discrete operators. Finally in Subsection 3.5 we state the virtual element discrete problem.

### *3.1. Mesh assumptions*

From now on, we will denote with $P$ a general polyhedron having $\ell_V \in \mathbb{N}^+$ vertexes $V$, $\ell_e \in \mathbb{N}^+$ (possibly curved) edges $e$ and $\ell_f \in \mathbb{N}^+$ (possibly curved) faces $f$.

For each polyhedron $P$, each face $f$ of $P$ and each edge $e$ of $f$ we denote with:

- $\boldsymbol{n}_P^f$ (resp. $\boldsymbol{n}_P$) the unit outward normal vector to $f$ (resp. to $\partial P$),
- $\boldsymbol{\tau}_1^f$ and $\boldsymbol{\tau}_2^f$ two orthogonal unit vectors lying on the tangent plane to $f$ and such that $\boldsymbol{\tau}_1^f \wedge \boldsymbol{\tau}_2^f = \boldsymbol{n}_P^f$,
- $\boldsymbol{x}_f := (x_{f\,1}, x_{f\,2})$ the independent variable on $f$, i.e., a local coordinate system associated with the axes $\boldsymbol{\tau}_f^1$ and $\boldsymbol{\tau}_f^2$.
- $\overline{\boldsymbol{x}}_P$, $h_P$, $|P|$, the centroid, the diameter and the measure of $P$ respectively, $h_e$ the length of $e$.

Let $\Omega_h$ be a decomposition of $\Omega$ into polyhedrons $P$ completed along $\partial\Omega$ by curved elements whose boundary contains a portion of the surface $\partial\Omega$, and we define the mesh-size $h := \sup_{P\in\Omega_h} h_P$. We denote by $\mathcal{F}_h$ the set of all the mesh faces divided into internal $\mathcal{F}_h^{\text{int}}$ and external $\mathcal{F}_h^{\text{ext}}$ faces; the latter is split into "essential faces" $\mathcal{F}_h^{\partial_e\Omega}$ and "natural faces" $\mathcal{F}_h^{\partial_n\Omega}$. For any $P \in \Omega_h$ we denote by $\mathcal{F}_h^P$ the set of the faces of $P$.

With a slight abuse of notation, we define the following maps to deal with both flat and curved faces:

- for any curved face $f \in \mathcal{F}_h$, we denote with $\gamma\colon \mathfrak{f} \subset \mathfrak{F} \to f$ the restriction of $\gamma\colon \mathfrak{F} \to \partial\Omega$ having image $f$,
- for any flat face $f \in \mathcal{F}_h$ we denote by $\gamma\colon \mathfrak{f} \to f$ the map $\boldsymbol{x}_f \mapsto \boldsymbol{x}$.

Finally we denote with $\boldsymbol{x}_\mathfrak{f} := (x_{\mathfrak{f}\,1}, x_{\mathfrak{f}\,2})$ the coordinate system on $\mathfrak{f}$ and with $\overline{\boldsymbol{x}}_\mathfrak{f}$, $h_\mathfrak{f}$, $|\mathfrak{f}|$ the centroid, the diameter and the measure of $\mathfrak{f}$. We make the following assumption on the mesh.

**Assumption 2 (Mesh assumptions).** *For all $h$, each element $P$ in $\Omega_h$ is a contractible polyhedron that fulfils the following properties:*

- *$P$ is star-shaped with respect to a ball $B_P$ of radius $\geq \rho\, h_P$,*
- *for every face $f$ of $P$, the parameter space $\mathfrak{f}$ associated to $f$ is star-shaped with respect to a disk $B_\mathfrak{f}$ of radius $\geq \rho\, h_P$,*
- *every edge $e$ in $P$ satisfies $h_e \geq \rho\, h_P$,*

*where $\rho$ is a uniform positive constant.*

The total number of vertexes, edges, faces and elements in the decomposition $\Omega_h$ are denoted respectively with $L_V$, $L_e$, $L_f$, $L_P$.

**Remark 3.** *Virtual element methods naturally handle hanging nodes [31], as a conseguence the present method can also deal with them on curved faces.*

*3.2. Polynomial and mapped polynomial spaces*

Using standard VEM notations, for any $n \in \mathbb{N}$ and for any mesh object (polyhedron, face, edge) $\mathcal{O} \subset \mathbb{R}^3$ the space $\mathbb{P}_n(\mathcal{O})$ denotes the set of polynomials on $\mathcal{O}$ of degree lower or equal to $n$. Moreover, for any $d = 1, 2, 3$ we define

$$\pi_{n,d} := \dim(\mathbb{P}_n(\mathbb{R}^d))\,. \tag{3}$$

For any $n \in \mathbb{N}$ and $s \in \mathbb{R}^+$ let us introduce the spaces:

- $\mathbb{P}_n(\Omega_h) := \{q \in L^2(\Omega_h) : q_{|P} \in \mathbb{P}_n(P)\ \forall P \in \Omega_h\}$,
- $H^s(\Omega_h) := \{v \in L^2(\Omega_h) : v_{|P} \in H^s(P)\ \forall P \in \Omega_h\}$ equipped with the broken norm and seminorm

$$\|v\|^2_{s,\Omega_h} := \sum_{P\in\Omega_h} \|v\|^2_{s,P}\,, \qquad |v|^2_{s,\Omega_h} := \sum_{P\in\Omega_h} |v|^2_{s,P}\,.$$

Note that on each polyhedron $P$ the following useful polynomial decompositions hold [25]

$$[\mathbb{P}_n(P)]^3 = \nabla(\mathbb{P}_{n+1}(P)) \oplus (\boldsymbol{x} \wedge [\mathbb{P}_{n-1}(P)]^3)\,, \tag{4}$$

$$[\mathbb{P}_n(P)]^3 = \mathbf{curl}(\mathbb{P}_{n+1}(P)) \oplus \boldsymbol{x}\, \mathbb{P}_{n-1}(P)\,. \tag{5}$$

A natural basis associated with the space $\mathbb{P}_n(P)$ is the set of normalized monomials

$$\mathcal{M}_n(P) := \left\{ \left( \frac{\boldsymbol{x} - \overline{\boldsymbol{x}}_P}{h_E} \right)^{\boldsymbol{\beta}} \text{ with } |\boldsymbol{\beta}| \leq n \right\}$$

where $\boldsymbol{\beta}$ is a 3d multi-index. Notice that $\|m\|_{L^\infty(P)} \leq 1$ for any $m \in \mathcal{M}_n(P)$. We extend the basis $\mathcal{M}_n(P)$ for vector valued polynomials $[\mathbb{P}_n(P)]^3$ defining

$$\boldsymbol{\mathcal{M}}_n(P) := \left\{(m_r, 0, 0)^\top,\ (0, m_s, 0)^\top,\ (0, 0, m_t)^\top \text{ with } m_r, m_s, m_t \in \mathcal{M}_n(P)\right\}.$$

Let us now introduce the polynomial spaces on the faces $f \in \mathcal{F}_h$. Following the same approach in [17], let $\mathfrak{f} \subset \mathbb{R}^2$ be the parameter space associated with $f$, then we denote by $\mathbb{P}_n(\mathfrak{f})$ the set of polynomials on $\mathfrak{f}$ of degree $\leq n$ with the associated basis of normalized polynomials

$$\mathcal{M}_n(\mathfrak{f}) := \left\{ \left( \frac{\boldsymbol{x}_\mathfrak{f} - \overline{\boldsymbol{x}}_\mathfrak{f}}{h_\mathfrak{f}} \right)^{\boldsymbol{\alpha}} \text{ with } |\boldsymbol{\alpha}| \leq n \right\}$$

where $\boldsymbol{\alpha}$ is a 2d multi-index. Again we notice that $\|m\|_{L^\infty(\mathfrak{f})} \leq 1$ for any $m \in \mathcal{M}_n(\mathfrak{f})$. For each face $f \in \mathcal{F}_h$ we consider the following mapped polynomial and scaled monomial spaces

$$\widetilde{\mathbb{P}}_n(f) := \{\widetilde{q} = q \circ \gamma^{-1} : q \in \mathbb{P}_n(\mathfrak{f})\}, \qquad \widetilde{\mathcal{M}}_n(f) := \{\widetilde{m} = m \circ \gamma^{-1} : m \in \mathcal{M}_n(\mathfrak{f})\},$$

i.e., $\widetilde{\mathbb{P}}_n(f)$ is made of all functions that are polynomials with respect to the parametrization $\gamma$. It is important to note that the following property holds:

**Property 1.** *For any face $f \in \mathcal{F}_h^P$ we have $\mathbb{P}_n(P)|_f \subset \widetilde{\mathbb{P}}_n(f)$ if $f$ is flat, or $\mathbb{P}_0(P)|_f \subset \widetilde{\mathbb{P}}_n(f)$ and in general $\mathbb{P}_i(P)|_f \not\subset \widetilde{\mathbb{P}}_n(f)$, for $i > 0$, if $f$ is curved. The same considerations apply to $\widetilde{\mathcal{M}}_n(f)$.*

The local $L^2$-projection operator $\boldsymbol{\Pi}_n^{0,P} \colon [L^2(P)]^3 \to [\mathbb{P}_n(P)]^3$ is defined as follows: for any $\boldsymbol{w} \in [L^2(P)]^3$ we have

$$\int_P \boldsymbol{\Pi}_n^{0,P} \boldsymbol{w} \cdot \boldsymbol{m} \, \mathrm{d}P = \int_P \boldsymbol{w} \cdot \boldsymbol{m} \, \mathrm{d}P \quad \forall \boldsymbol{m} \in \boldsymbol{\mathcal{M}}_n(P). \tag{6}$$

We denote by $\boldsymbol{\Pi}_n^0 \colon [L^2(\Omega)]^3 \to [\mathbb{P}_n(\Omega_h)]^3$ the projection onto the space of piecewise polynomials defined element-wise by $(\boldsymbol{\Pi}_n^0 \boldsymbol{w})|_P := \boldsymbol{\Pi}_n^{0,P}(\boldsymbol{w}|_P)$ for all $P \in \Omega_h$. Similarly the $L^2$-face projection operator $\widetilde{\Pi}_n^{0,f} \colon L^2(f) \to \widetilde{\mathbb{P}}_n(f)$ is defined as follows: for any $w \in L^2(f)$

$$\int_f \widetilde{\Pi}_n^{0,f} w \, \widetilde{m} \, \mathrm{d}f = \int_f w \, \widetilde{m} \, \mathrm{d}f \quad \forall \widetilde{m} \in \widetilde{\mathcal{M}}_n(f). \tag{7}$$

In the following the symbol $\lesssim$ will denote a bound up to a generic positive constant, independent of the mesh size $h$, but which may depend on $\Omega$, on the "polynomial" order $k$, on the parametrization $\gamma$ in Assumption 1 and on the shape constant $\rho$ in Assumptions 2.

### *3.3. Virtual Element Spaces*

In this subsection we present the discrete spaces for velocity and pressure. The idea behind the construction of these approximation spaces is simple and effective: the normal component of a virtual velocity function restricted on a curved face is still a polynomial but in the parameter space. The geometry is plugged in the virtual element space so it is perfectly matched by any virtual function. The proposed construction extends to the 3d case the 2d curved space defined in [17].

**Remark 4.** *A standard virtual element space used to solve a Laplacian problem has virtual functions on each polyhedron face [5, 7]. Having Problem 2 in mixed form avoids this difficulty since on faces we have polynomials, see Equation* (8)*.*

Given a polyhedron $P$ that can have one or more curved faces, we define the local space $\boldsymbol{\mathcal{V}}_h^k(P)$ as

$$\begin{aligned}\boldsymbol{\mathcal{V}}_h^k(P) := \big\{ \boldsymbol{v}_h \in H(\mathrm{div}\,,P) \cap H(\mathbf{curl}\,,P) \,:\, &(i)\ \ \mathrm{div}\,\boldsymbol{v}_h \in \mathbb{P}_{k-1}(P),\\ &(ii)\ \ \mathbf{curl}\,\boldsymbol{v}_h \in \mathbf{curl}([\mathbb{P}_k(P)]^3),\\ &(iii)\ \ \boldsymbol{v}_h\cdot\boldsymbol{n}_f \in \widetilde{\mathbb{P}}_k(f)\,\forall f\in\mathcal{F}_h^P\big\}\,.\end{aligned} \tag{8}$$

We here summarize the main properties of the space $\boldsymbol{\mathcal{V}}_h^k(P)$, we refer to [25, 17] for a deeper analysis.

**Property 2 (Polynomial inclusion).** *Differently from the standard case with flat faces, in general* $[\mathbb{P}_k(P)]^3 \not\subseteq \boldsymbol{\mathcal{V}}_h^k(P)$*, but it holds that* $[\mathbb{P}_0(P)]^3 \subseteq \boldsymbol{\mathcal{V}}_h^k(P)$

**Property 3 (Degrees of Freedom).** *The following linear operators constitute a set of DoFs for* $\boldsymbol{\mathcal{V}}_h^k(P)$*:*

- ***normal face moments:*** *for each face* $F\in\mathcal{F}_h^P$ *the moments*

$$\frac{1}{|\mathfrak{f}|}\int_f (\boldsymbol{v}_h\cdot\boldsymbol{n}_f^P)\,\widetilde{m}_k\,\mathrm{d}f \quad \forall \widetilde{m}_k\in\widetilde{\mathcal{M}}_k(f)\,;$$

- ***divergence moments:*** *the bulk moments*

$$\frac{h_P}{|P|}\int_P (\mathrm{div}\,\boldsymbol{v}_h)\,m_{k-1}\,\mathrm{d}P\,, \quad \forall m_{k-1}\in\mathcal{M}_{k-1}(P)\backslash\mathcal{M}_0(P)\,;$$

- ***internal cross moments:*** *the bulk moments*

$$\frac{1}{|P|}\int_P \boldsymbol{v}_h\cdot(\boldsymbol{m}_I\wedge\boldsymbol{m}_{k-1})\,\mathrm{d}P\,, \quad \forall \boldsymbol{m}_{k-1}\in\boldsymbol{\mathcal{M}}_k(P)\,,$$

  *where* $\boldsymbol{m}_I := (\boldsymbol{x}-\overline{\boldsymbol{x}}_P)/h_P$*.*

*Therefore, recalling* (4)*, the dimension of* $\boldsymbol{\mathcal{V}}_h^k(P)$ *is*

$$\dim(\boldsymbol{\mathcal{V}}_h^k(P)) = \pi_{k,2}\,\ell_f + 3\pi_{k,3} + \pi_{k-1,3} - \pi_{k+1,3}\,.$$

**Property 4 (Divergence operator & Polynomial projection).** *The DoFs allow us to compute*

$$\mathrm{div}\colon \boldsymbol{\mathcal{V}}_h^k(P)\to\mathbb{P}_{k-1}(P) \qquad \textit{and} \qquad \boldsymbol{\Pi}_k^{0,P}\colon \boldsymbol{\mathcal{V}}_h^k(P)\to[\mathbb{P}_k(P)]^3\,.$$

The global virtual element velocities space is defined by

$$\boldsymbol{\mathcal{V}}_h^k(\Omega_h) := \{\boldsymbol{v}_h \in \boldsymbol{V} \ : \ \boldsymbol{v}_h|_P \in \boldsymbol{\mathcal{V}}_h^k(P) \, \forall P \in \Omega_h\} \tag{9}$$

whose dimension is

$$\dim(\boldsymbol{\mathcal{V}}_h^k(\Omega_h)) = \pi_{k,2} \, L_f + (3\pi_{k,3} + \pi_{k-1,3} - \pi_{k+1,3}) \, L_P \, .$$

The global pressure variable $p$ is approximated via element-wise polynomials of degree $k-1$, i.e.,

$$Q_h^k(\Omega_h) := \left\{ v \in L^2(\Omega) \ : \ v|_P \in \mathbb{P}_{k-1}(P) \, \forall P \in \Omega_h \right\} \, . \tag{10}$$

The corresponding DoFs are chosen, defining

- **pressure moments:** for any $P \in \Omega_h$

$$\frac{1}{|P|} \int_P v \, m_{k-1} \, \mathrm{d}P \quad \forall m_{k-1} \in \mathcal{M}_{k-1}(P) \, .$$

*3.4. Virtual Element Forms*

The next step in the construction of our method is to define a discrete version of the continuous bilinear form $a(\cdot,\cdot)$ in (1) and the linear form $G(\cdot)$ in (2). It is clear that for an arbitrary function in $\boldsymbol{\mathcal{V}}_h^k(\Omega_h)$ the forms are not computable since the discrete functions are not known in closed form. Therefore, following the usual VEM procedure, we need to construct discrete forms that are computable by the DoFs. Notice that, on the basis of Property 4 and the definition of the pressures space (10), the bilinear form $b(\cdot,\cdot)$ can be exactly computed by the DoFs.

In the light of Property 4, on each polyhedron $P \in \Omega_h$, we define the computable local discrete form: $\forall \boldsymbol{v}_h, \boldsymbol{w}_h \in \boldsymbol{\mathcal{V}}_h^k(P)$

$$a_h^P(\boldsymbol{v}_h, \boldsymbol{w}_h) := \int_P \lambda \, \boldsymbol{\Pi}_k^{0,P} \boldsymbol{v}_h \, \boldsymbol{\Pi}_k^{0,P} \boldsymbol{w}_h \, \mathrm{d}P + \mathcal{S}^P(\boldsymbol{T}_k^{0,P} \boldsymbol{v}_h, \boldsymbol{T}_k^{0,P} \boldsymbol{w}_h) \, , \tag{11}$$

where $\boldsymbol{T}_k^{0,P} = \boldsymbol{I} - \boldsymbol{\Pi}_k^{0,P}$. The VEM stabilizing term in (11) here proposed is the so-called `dofi-dofi` stabilization [7, 17] given by

$$\mathcal{S}^P(\boldsymbol{v}_h, \boldsymbol{w}_h) := \|\lambda\|_{L^\infty(P)} |P| \sum_{i=1}^{\#\mathtt{dof}} \mathtt{dof}_i\big(\boldsymbol{v}_h\big) \mathtt{dof}_i\big(\boldsymbol{w}_h\big) \, , \tag{12}$$

where $\#\mathtt{dof}$ is the number of degrees of freedom associated with the polyhedron $P$ and the function $\mathtt{dof}_i$ returns the $i^{\text{th}}$ DoFs value.

We define the global approximated bilinear form $a_h(\cdot,\cdot)\colon \boldsymbol{\mathcal{V}}_h^k(\Omega_h) \times \boldsymbol{\mathcal{V}}_h^k(\Omega_h) \to \mathbb{R}$ by simply summing each local contribution:

$$a_h(\boldsymbol{v}_h, \boldsymbol{w}_h) := \sum_{P \in \Omega_h} a_h^P(\boldsymbol{v}_h, \boldsymbol{w}_h) \qquad \forall \boldsymbol{v}_h, \boldsymbol{w}_h \in \boldsymbol{\mathcal{V}}_h^k(\Omega_h) \, . \tag{13}$$

The last step consists in constructing a computable approximation of the form $G(\cdot)$ in (2). Employing again Property 4 we define

$$G_h(\boldsymbol{v}_h) := -(\overline{p}, \boldsymbol{v}_h \cdot \boldsymbol{n})_{\partial_n \Omega} + (\kappa^{-1} \boldsymbol{g}, \boldsymbol{\Pi}_k^0 \boldsymbol{v}_h)_\Omega \qquad \forall \boldsymbol{v}_h \in \boldsymbol{\mathcal{V}}_h^k(\Omega_h) \, . \tag{14}$$

**Remark 5.** *In definitions* (11) *and* (14) *we are tacitly assuming that we are able to compute the integrals of polynomials on curved polyhedrons and on curved faces with a given parametrization* $\gamma$*. A description of the adopted integration rules can be found in Section 5.*

### *3.5. Virtual Element Problem*

We are now ready to state the proposed discrete version of Problem 2. Referring to the spaces (9) and (10), the forms (13) and (14), we consider the virtual element problem

**Problem 3 (Darcy problem - VEM scheme).** *Find* $(\boldsymbol{q}_h, p_h) \in \boldsymbol{\mathcal{V}}_h^k(\Omega_h) \times Q_h^k(\Omega_h)$ *such that*

$$\begin{cases} a_h(\boldsymbol{q}_h, \boldsymbol{v}_h) + b(\boldsymbol{v}_h, p_h) = G_h(\boldsymbol{v}_h) & \forall \boldsymbol{v}_h \in \boldsymbol{\mathcal{V}}_h^k(\Omega_h)\,, \\ b(\boldsymbol{q}_h, v_h) = F(v_h) & \forall v_h \in Q_h^k(\Omega_h)\,. \end{cases}$$

We stress that if the domain $\Omega$ is a polyhedron with flat faces, i.e., if $\partial\Omega$ is made up of a finite number of flat faces, we recover the "straight" $H(\mathrm{div})$-conforming VEM presented in [25].

## 4. Theoretical analysis

In the present section we establish the optimal approximation properties for the curved virtual element space (9), and we derive the inf-sup stability of Problem 3.

We start by reviewing a classical approximation result for polynomials on star-shaped domains, see for instance [38].

**Lemma 1 (Bramble-Hilbert).** *Referring to* (6)*, let* $0 \le m \le s \le k+1$*, under Assumption 2 for all* $\boldsymbol{v} \in \boldsymbol{V} \cap [H^s(\Omega_h)]^3$ *it holds*

$$|\boldsymbol{v} - \boldsymbol{\Pi}_k^0 \boldsymbol{v}|_{m,\Omega_h} \lesssim h^{s-m}\, |\boldsymbol{v}|_{s,\Omega_h}\,.$$

Let us introduce the linear Fortin operator $\boldsymbol{\Pi}_k^{\mathrm{F}} \colon [H^1(\Omega)]^3 \to \boldsymbol{\mathcal{V}}_h^k(\Omega_h)$ defined for any $\boldsymbol{w} \in [H^1(\Omega)]^3$ by

$$\int_f (\boldsymbol{w} - \boldsymbol{\Pi}_k^{\mathrm{F}} \boldsymbol{w}) \cdot \boldsymbol{n}^f\, \widetilde{m}_i \,\mathrm{d}f = 0 \qquad \forall \widetilde{m}_i \in \widetilde{\mathcal{M}}_k(f); \tag{15}$$

$$\int_P \mathrm{div}(\boldsymbol{w} - \boldsymbol{\Pi}_k^{\mathrm{F}} \boldsymbol{w})\, m_j \,\mathrm{d}P = 0 \qquad \forall m_j \in \mathcal{M}_{k-1}(P) \setminus \mathcal{M}_0(P); \tag{16}$$

$$\int_E \mathbf{curl}(\boldsymbol{w} - \boldsymbol{\Pi}_k^{\mathrm{F}} \boldsymbol{w}) \cdot \mathbf{curl}\, \boldsymbol{m_l} \,\mathrm{d}P = 0 \qquad \forall \boldsymbol{m_l} \in \boldsymbol{\mathcal{M}}_k(P), \tag{17}$$

for all $f \in \mathcal{F}_h$ and $P \in \Omega_h$. The definition above easily implies that the following diagram is commutative

$$\begin{array}{ccccc} [H^1(\Omega)]^3 & \xrightarrow{\text{div}} & Q & \xrightarrow{0} & 0 \\ \Big\downarrow \boldsymbol{\Pi}_k^{\mathrm{F}} & & \Big\downarrow \Pi_{k-1}^0 & & \\ \boldsymbol{\mathcal{V}}_h^k(\Omega_h) & \xrightarrow{\text{div}} & Q_h^k(\Omega_h) & \xrightarrow{0} & 0 \end{array} \tag{18}$$

where the right arrows in this diagram indicate that the divergence operator is surjective. In particular, employing (15) coupled with Property 1 and (16), we have the following property:

$$\operatorname{div}(\boldsymbol{\Pi}_k^{\mathrm{F}} \boldsymbol{w}) = \Pi_{k-1}^0 \operatorname{div} \boldsymbol{w} \quad \forall \boldsymbol{w} \in [H^1(\Omega)]^3. \tag{19}$$

As a consequence of the above arguments we have two results. The first one deals with the approximation property of the space (9), while the second one is associated with the exactness of the sequence (18) and deals with the inf-sup stability of the method [24].

**Proposition 1.** *Let $\boldsymbol{w} \in \boldsymbol{V} \cap [H^{k+1}(\Omega_h)]^3$ and let $\boldsymbol{\Pi}_k^{\mathrm{F}}$ be the linear Fortin operator. Then, under Assumption 2, the following estimates hold*

$$\| \operatorname{div} \boldsymbol{w} - \operatorname{div} \boldsymbol{\Pi}_k^{\mathrm{F}} \boldsymbol{w} \|_{0,\Omega} \lesssim h^k \, | \operatorname{div} \boldsymbol{w} |_{k,\Omega_h} \, , \tag{20}$$

$$\| \boldsymbol{w} - \boldsymbol{\Pi}_k^{\mathrm{F}} \boldsymbol{w} \|_{0,\Omega} \lesssim h^{k+1} \, \| \boldsymbol{w} \|_{k+1,\Omega_h} \, . \tag{21}$$

**Proof 1.** *The estimate* (20) *is a direct consequence of* (19) *and Lemma 1. Concerning the $L^2$ estimate, we recall (see [39, Corollary 3.2]) that any function $\boldsymbol{v} \in H(\operatorname{div}, P) \cap H(\mathbf{curl}, P)$ can be decomposed as*

$$\boldsymbol{v} = \nabla \phi - \mathbf{curl} \, \boldsymbol{\psi} \tag{22}$$

*where $\phi$ and $\boldsymbol{\psi}$ are defined by*

$$\begin{cases} \Delta \phi = \operatorname{div} \boldsymbol{v} & \text{in } P, \\ \nabla \phi \cdot \boldsymbol{n}^P = \boldsymbol{v} \cdot \boldsymbol{n}^P & \text{on } \partial P, \end{cases} \qquad \text{and} \qquad \begin{cases} \boldsymbol{\Delta} \boldsymbol{\psi} = \mathbf{curl} \, \boldsymbol{v} & \text{in } P, \\ \operatorname{div} \boldsymbol{\psi} = 0 & \text{in } P, \\ \boldsymbol{\psi} \times \boldsymbol{n}^P = \mathbf{0} & \text{on } \partial P, \end{cases} \tag{23}$$

*and $\phi$ is zero averaged. Moreover, the decomposition* (22) *is $L^2$-orthogonal, i.e.,*

$$\| \boldsymbol{v} \|_{0,P}^2 = \| \nabla \phi \|_{0,P}^2 + \| \mathbf{curl} \, \boldsymbol{\psi} \|_{0,P}^2 \, . \tag{24}$$

*Let $\boldsymbol{w} \in [H^{k+1}(\Omega_h)]$ and let $\boldsymbol{\Pi}_k^{\mathrm{F}} \boldsymbol{w} \in \boldsymbol{\mathcal{V}}_h^k(\Omega_h)$ be its interpolant function defined by* (15), (16) *and* (17). *Then on each $P \in \Omega_h$ consider the $L^2$-orthogonal decomposition*

$$\boldsymbol{w} - \boldsymbol{\Pi}_k^{\mathrm{F}} \boldsymbol{w} = \nabla \delta_h - \mathbf{curl} \, \boldsymbol{\mu}_h \tag{25}$$

*where (the zero averaged function) $\delta_h$ and $\boldsymbol{\mu}_h$ are defined by*

$$\begin{cases} \Delta\delta_h = (I - \Pi_{k-1}^{0,P}) \operatorname{div} \boldsymbol{w} & \text{in } P, \\ \nabla\delta_h \cdot \boldsymbol{n}_f^P = (I - \widetilde{\Pi}_k^{0,f})\boldsymbol{w} \cdot \boldsymbol{n}_f^P \quad \forall f \in \mathcal{F}_h^P, \end{cases} \quad \begin{cases} \boldsymbol{\Delta}\boldsymbol{\mu}_h = \mathbf{curl}(\boldsymbol{w} - \boldsymbol{\Pi}_k^{\mathrm{F}}\boldsymbol{w}) & \text{in } P, \\ \operatorname{div}\boldsymbol{\mu}_h = 0 & \text{in } P, \\ \boldsymbol{\mu}_h \times \boldsymbol{n}^P = \mathbf{0} & \text{on } \partial P. \end{cases} \tag{26}$$

*We now estimate each term in the decomposition* (25)*. Let us analyse the first term. Integrating by parts from* (26) *we infer*

$$\begin{aligned} \|\nabla\delta_h\|_{0,P}^2 &= -\int_P (I - \Pi_{k-1}^{0,P}) \operatorname{div} \boldsymbol{w}\, \delta_h \,\mathrm{d}P + \sum_{f \in \mathcal{F}_h^P} \int_f (I - \widetilde{\Pi}_k^{0,f})\boldsymbol{w} \cdot \boldsymbol{n}_f^P\, \delta_h \,\mathrm{d}f \\ &\le \|(I - \Pi_{k-1}^{0,P}) \operatorname{div} \boldsymbol{w}\|_{0,P} \|\delta_h\|_{0,E} + \sum_{f \in \mathcal{F}_h^P} \|(I - \widetilde{\Pi}_k^{0,f})\boldsymbol{w} \cdot \boldsymbol{n}_f^P\|_{0,f} \|\delta_h\|_{0,f} \\ &=: \sigma_1 + \sigma_2 \,. \end{aligned} \tag{27}$$

*Employing Lemma 1 and a scaled Poincaré inequality for the zero averaged function $\delta_h$ we derive*

$$\sigma_1 = \|(I - \Pi_{k-1}^{0,P}) \operatorname{div} \boldsymbol{w}\|_{0,P} \|\delta_h\|_{0,P} \lesssim h_E^{k+1} |\operatorname{div} \boldsymbol{w}|_{k,P} \, \|\nabla\delta_h\|_{0,P} \,. \tag{28}$$

*For the boundary term $\sigma_2$, applying the Cauchy-Schwartz inequality, a scaled trace inequality and again a scaled Poincaré inequality we get*

$$\begin{aligned} \sigma_2 &= \|\delta_h\|_{0,\partial E} \bigg( \sum_{f \in \mathcal{F}_h^P} \|(I - \widetilde{\Pi}_k^{0,f})\boldsymbol{w} \cdot \boldsymbol{n}_f^P\|_{0,f}^2 \bigg)^{1/2} \\ &\lesssim (h_P^{-1/2} \|\delta_h\|_{0,P} + h_P^{1/2} \|\nabla\delta_h\|_{0,P}) \bigg( \sum_{f \in \mathcal{F}_h^P} \|(I - \widetilde{\Pi}_k^{0,f})\boldsymbol{w} \cdot \boldsymbol{n}_f^P\|_{0,f}^2 \bigg)^{1/2} \\ &\lesssim h_P^{1/2} \|\nabla\delta_h\|_{0,P} \bigg( \sum_{f \in \mathcal{F}_h^P} \|(I - \widetilde{\Pi}_k^{0,f})\boldsymbol{w} \cdot \boldsymbol{n}_f^P\|_{0,f}^2 \bigg)^{1/2} . \end{aligned}$$

*We observe that from Assumption 1 and Lemma 2.3 in [40] it holds that $\boldsymbol{w} \cdot \boldsymbol{n}_f^P \in H^{k+1/2}(f)$. Moreover, employing the same argument in the proof of Lemma 3.2 in [16] (combined with Lemma 2.2 and Lemma 2.3 in [40]), we infer*

$$\|(I - \widetilde{\Pi}_k^{0,f})\boldsymbol{w} \cdot \boldsymbol{n}_f^P\|_{0,f} \lesssim h_P^{k+1/2} \|\boldsymbol{w} \cdot \boldsymbol{n}_f^P\|_{k+1/2,f} \lesssim h_P^{k+1/2} \|\boldsymbol{w}\|_{k+1/2,f} \,.$$

*Applying a scaled trace inequality and again a scaled Poincaré inequality, from the previous bound we get*

$$\sigma_2 \lesssim h_P^{k+1} \|\nabla\delta_h\|_{0,P} \|\boldsymbol{w}\|_{k+1/2,\partial P} \lesssim h_P^{k+1} \|\nabla\delta_h\|_{0,P} \|\boldsymbol{w}\|_{k+1,P} \,. \tag{29}$$

*Combining* (28) *and* (29) *in* (27) *we obtain*

$$\|\nabla\delta_h\|_{0,P} \lesssim h_P^{k+1} \|\boldsymbol{w}\|_{k+1,P} \,. \tag{30}$$

*Concerning the term* $\mathbf{curl}\,\boldsymbol{\mu}_h$*, from* (26) *we have*

$$\|\mathbf{curl}\,\boldsymbol{\mu}_h\|_{0,P}^2 = -\int_P \boldsymbol{\Delta}\boldsymbol{\mu}_h \cdot \boldsymbol{\mu}_h \,\mathrm{d}P = -\int_P \mathbf{curl}(\boldsymbol{w} - \boldsymbol{\Pi}_k^{\mathrm{F}}\boldsymbol{w}) \cdot \boldsymbol{\mu}_h \,\mathrm{d}P\,. \tag{31}$$

*Notice now that from* (5)*, there exists* $\boldsymbol{p}_1 \in [\mathbb{P}_1(P)]^3$ *such that* $\boldsymbol{\Pi}_0^{0,P}\boldsymbol{\mu}_h = \mathbf{curl}\,\boldsymbol{p}_1$*. Therefore from* (17) *and* (31) *we infer*

$$\begin{aligned}\|\mathbf{curl}\,\boldsymbol{\mu}_h\|_{0,P}^2 &= -\int_P \mathbf{curl}(\boldsymbol{w} - \boldsymbol{\Pi}_k^{\mathrm{F}}\boldsymbol{w}) \cdot (\boldsymbol{\mu}_h - \boldsymbol{\Pi}_0^{0,P}\boldsymbol{\mu}_h)\,\mathrm{d}P \\ &\leq \|\mathbf{curl}(\boldsymbol{w} - \boldsymbol{\Pi}_k^{\mathrm{F}}\boldsymbol{w})\|_{0,P}\|\boldsymbol{\mu}_h - \boldsymbol{\Pi}_0^{0,P}\boldsymbol{\mu}_h\|_{0,P} =: \tau_1\,\tau_2\,.\end{aligned} \tag{32}$$

*Employing Lemma 1 and Theorem 3.7 in [39], the term* $\tau_1$ *can be estimated as follows*

$$\tau_1 \lesssim h_P\|\boldsymbol{\nabla}\boldsymbol{\mu}_h\|_{0,P} \lesssim h_P\|\mathbf{curl}\,\boldsymbol{\mu}_h\|_{0,P}\,. \tag{33}$$

*For the term* $\tau_2$*, recalling* (17)*, we have*

$$\begin{aligned}\tau_2^2 = \|\mathbf{curl}(\boldsymbol{w} - \boldsymbol{\Pi}_k^{\mathrm{F}}\boldsymbol{w})\|_{0,P}^2 &= \int_P \mathbf{curl}(\boldsymbol{w} - \boldsymbol{\Pi}_k^{\mathrm{F}}\boldsymbol{w}) \cdot \mathbf{curl}(\boldsymbol{w} - \boldsymbol{\Pi}_k^{\mathrm{F}}\boldsymbol{w})\,\mathrm{d}P \\ &= \int_P \mathbf{curl}(\boldsymbol{w} - \boldsymbol{\Pi}_k^{\mathrm{F}}\boldsymbol{w}) \cdot \mathbf{curl}(\boldsymbol{w} - \boldsymbol{\Pi}_k^{0,P}\boldsymbol{w})\,\mathrm{d}P \\ &\leq \|\mathbf{curl}(\boldsymbol{w} - \boldsymbol{\Pi}_k^{\mathrm{F}}\boldsymbol{w})\|_{0,P}|\boldsymbol{w} - \boldsymbol{\Pi}_k^{0,P}\boldsymbol{w}|_{1,P}\,,\end{aligned}$$

*and then from Lemma 1 we obtain*

$$\tau_2 \lesssim h_P^k|\boldsymbol{w}|_{k+1,P}\,. \tag{34}$$

*From* (33) *and* (34) *we conclude*

$$\|\mathbf{curl}\,\boldsymbol{\mu}_h\|_{0,P} \lesssim h_P^{k+1}|\boldsymbol{w}|_{k+1,P}\,. \tag{35}$$

*The thesis now follows by collecting* (30) *and* (35) *in the* $L^2$*-orthogonal decomposition* (25)*.*

Finally, as a consequence of the diagram (18) we can state the following result (for the proof we refer to Theorem 4.2 and Corollary 4.3 in [6]).

**Proposition 2.** *Under Assumption 2, there exists* $\beta > 0$ *such that*

$$\inf_{v \in Q_h^k(\Omega_h)} \sup_{\boldsymbol{w} \in \boldsymbol{\mathcal{V}}_h^k(\Omega_h)} \frac{b(\boldsymbol{w}, v)}{\|v\|_Q\|\boldsymbol{w}\|_{\boldsymbol{V}}} \geq \beta\,.$$

**Remark 6.** *A technical important step in the theoretical analysis of the scheme is the derivation of the stability bounds*

$$\begin{aligned}&\|\boldsymbol{v}_h\|_{0,P}^2 \lesssim \mathcal{S}^P(\boldsymbol{v}_h, \boldsymbol{v}_h) && \text{for all } \boldsymbol{v}_h \in \boldsymbol{\mathcal{V}}_h^k(P), \\ &\|\boldsymbol{v}_h\|_{0,P}^2 \gtrsim \mathcal{S}^P(\boldsymbol{v}_h, \boldsymbol{v}_h) && \text{for all } \boldsymbol{v}_h \in \boldsymbol{\mathcal{V}}_h^k(P) + [\mathbb{P}_k(P)]^3,\end{aligned}$$

*for the stabilizing form* $\mathcal{S}^P(\cdot,\cdot)$ *in* (12)*. The theoretical analysis in principle can follow the same path of the 2d case [17].*

## 5. Integration over curved Polyhedrons

In this section we explain how we compute integrals inside polyhedrons characterized by curved faces. Fist, we describe how to integrate over curved faces. Then, we show how we extend the idea proposed in [35] from curved polygons to polyhedrons with curved faces.

### *5.1. Integration over curved 2d polygons*

We consider a curved face $f$ of a polyhedron $P$ and we make the same assumptions on definition, existence and regularity on the map $\gamma$, see the final part of Section 2 and Section 3.

Given any function $\psi$ defined over the face $f$, to integrate it we exploit the following formula:

$$\begin{aligned}\int_f \psi(\boldsymbol{x})\ \mathrm{d}f(\boldsymbol{x}) &= \int_{\mathfrak{f}} \widetilde{\psi}(\boldsymbol{x}_{\mathfrak{f}}) \left\| \frac{\partial \gamma}{\partial x_{\mathfrak{f}_1}} \times \frac{\partial \gamma}{\partial x_{\mathfrak{f}_2}}(\boldsymbol{x}_{\mathfrak{f}}) \right\| \ \mathrm{d}\mathfrak{f}(\boldsymbol{x}_{\mathfrak{f}}) \\ &\approx \sum_{i=1}^{n_{\mathfrak{f}}} \widetilde{\psi}(\boldsymbol{x}_{\mathfrak{f},i}) \left\| \frac{\partial \gamma}{\partial x_{\mathfrak{f}_1}} \times \frac{\partial \gamma}{\partial x_{\mathfrak{f}_2}}(\boldsymbol{x}_{\mathfrak{f},i}) \right\| \omega_{\mathfrak{f},i}\,,\end{aligned} \tag{36}$$

where $\widetilde{\psi}$ is the function $\psi$ written in terms of the parameter-space coordinate $\boldsymbol{x}_{\mathfrak{f}}$, $\left\| \frac{\partial \gamma}{\partial x_{\mathfrak{f}_1}} \times \frac{\partial \gamma}{\partial x_{\mathfrak{f}_2}} \right\|$ is the Jacobian of the transformation $\gamma$ and $\{\boldsymbol{x}_{\mathfrak{f},i}\}_{i=1}^{n_{\mathfrak{f}}}$ are the quadrature points in the parameter space $\mathfrak{f}$ and $\{\omega_{\mathfrak{f},i}\}_{i=1}^{n_{\mathfrak{f}}}$ are their corresponding weights.

From a more practical point of view the usage of (36) is not so straightforward. Indeed, one has to define the function $\widetilde{\psi}(\boldsymbol{x}_{\mathfrak{f}})$. However, to use the quadrature rule in (36) and avoid the definition of the function $\widetilde{\psi}$, we compute the physical quadrature points corresponding to the ones in the parameter space via the map $\gamma$

$$\left\{\boldsymbol{x}_{\mathfrak{f},i}\right\}_{i=1}^{n_{\mathfrak{f}}} \mapsto \left\{\boldsymbol{x}_i^f\right\}_{i=1}^{n_{\mathfrak{f}}},$$

and we modify (36) as

$$\int_f \psi(\boldsymbol{x})\ \mathrm{d}f(\boldsymbol{x}) \approx \sum_{i=1}^{n_{\mathfrak{f}}} \psi(\boldsymbol{x}_i^f) \left\| \frac{\partial \gamma}{\partial x_{\mathfrak{f}_1}} \times \frac{\partial \gamma}{\partial x_{\mathfrak{f}_2}}(\boldsymbol{x}_{\mathfrak{f},i}) \right\| \omega_{\mathfrak{f},i} \tag{37}$$

This quadrature rule does not depend on $\widetilde{\psi}$ so there is no need to create such a function. Moreover, such double quadrature point lists will play a key role in the computation of the volume quadrature presented in Section 5.2.

**Remark 7.** *Since the domain $\mathfrak{f} \subset \mathbb{R}^2$ in the parameter space may have curved boundaries, we exploit the integration strategy proposed in [35, 16].*

*5.2. Integration over curved 3d polyhedrons*

In this section we propose a quadrature rule to integrate a function inside polyhedrons characterized by curved faces. The proposed formula is an extension of the one proposed in [35].

Consider a function $\psi$ defined in a polyhedron $P$ and suppose that we would like to compute the integral

$$\int_P \psi(\boldsymbol{x}) \, \mathrm{dP} \, .$$

The idea is to move the computation of such integral to an integration over the polyhedron faces. To achieve this goal, we exploit the divergence theorem. We define a proper vectorial field $\boldsymbol{\Psi}$ such that

$$\operatorname{div} \boldsymbol{\Psi} = \psi \, .$$

One possible choice of such function is the vector field

$$\boldsymbol{\Psi}(x_1, \, x_2, \, x_3) = \begin{bmatrix} 0 \\ 0 \\ \displaystyle\int_{\overline{x}_3}^{x_3} \psi(x_1, \, x_2, \, t) \, \mathrm{dt} \end{bmatrix} ,$$

where $\overline{x}_3$ is the $x_3$-coordinate of the polyhedron barycentre. Starting from such vector field and exploiting the idea of (37), we obtain the following integration formula

$$\begin{aligned} \int_P \psi(\boldsymbol{x}) \, \mathrm{d}P = \int_P \operatorname{div} \boldsymbol{\Psi}(\boldsymbol{x}) \, \mathrm{d}P = \sum_{f \in \mathcal{F}_h^P} \int_f \boldsymbol{\Psi} \cdot \boldsymbol{n}_f^P(\boldsymbol{x}) \, \mathrm{d}f = \sum_{f \in \mathcal{F}_h^P} \int_f \Psi_3 \, n_{f,3}^P(\boldsymbol{x}) \, \mathrm{d}f \\ = \sum_{f \in \mathcal{F}_h^P} \sum_{i=1}^{n_\mathfrak{f}} \Psi_3 \, n_{f,3}^P(\boldsymbol{x}_i^f) \left\| \frac{\partial \gamma}{\partial x_{\mathfrak{f}_1}} \times \frac{\partial \gamma}{\partial x_{\mathfrak{f}_2}} (\boldsymbol{x}_{\mathfrak{f},i}) \right\| \omega_{\mathfrak{f},i} \end{aligned} \tag{38}$$

In the last expression we are able to compute all terms. Both $n_{f,3}^P$ and $\left\| \frac{\partial \gamma}{\partial x_{\mathfrak{f}_1}} \times \frac{\partial \gamma}{\partial x_{\mathfrak{f}_2}} \right\|$ are known functions since they describe the $x_3$-component of the normal to the surface geometry and the Jacobian of the map $\gamma$, respectively. Moreover, $\Psi_3$ is computable too. Indeed, recalling the definition of the vector field $\boldsymbol{\Psi}$, we evaluate such term via an edge integral:

$$\Psi_3(x_{1,i}^f, \, x_{2,i}^f, \, x_{3,i}^f) = \int_{\overline{x}_3}^{x_{3,i}^f} \psi(x_{1,i}^f, \, x_{2,i}^f, \, t) \, \mathrm{d}t \approx \sum_{j=1}^{m} \psi(x_{1,i}^f, \, x_{2,i}^f, \, x_{3,i,j}^f) \, \xi_{i,j} \, ,$$

where $\left\{ x_{3,i,j}^f \right\}_{j=1}^m$ and $\left\{ \xi_{i,j}^f \right\}_{j=1}^m$ are the nodes and the weights of a quadrature rule on the edges $[\overline{x}_3, \, x_{3,i}^f]$. Substituting the last equation in (38), we get the following integration formula:

$$\int_P \psi(\boldsymbol{x}) \, \mathrm{d}P \approx \sum_{f \in \mathcal{F}_h^P} \sum_{i=1}^{n_\mathfrak{f}} \sum_{j=1}^{m} \psi(x_{1,i}^f, \, x_{2,i}^f, \, x_{3,i,j}^f) \, \xi_{i,j} \, n_{f,3}^P(\boldsymbol{x}_i^f) \left\| \frac{\partial \gamma}{\partial x_{\mathfrak{f}_1}} \times \frac{\partial \gamma}{\partial x_{\mathfrak{f}_2}} (\boldsymbol{x}_{\mathfrak{f},i}) \right\| \omega_{\mathfrak{f},i} \, . \tag{39}$$

We can make the following observation about such formula. First of all it relies on some regularity assumptions for the polyhedron faces: they have to be defined via a map $\gamma$ that has to be at least $C^2$ since we exploit surface normals and the Jacobian.

The proposed quadrature rule has more than the expected number of quadrature points, which is not appealing from the computational point of view. However, we can use the procedure proposed in [36] to get a quadrature rule with the same order composed by a subset of the input points.

Such compression procedure is general and it is based on the resolution of a non-negative least squares problem that also ensures positivity of the weights. We apply such strategy to reduce the number of quadrature points in (39).

To show the effectiveness of the compression procedure, we consider the following example: a cube whose top face is a bilinear surface and a quadrature formula that exactly integrates polynomials of degree 2.

Figure 1 presents the resulting quadrature points. The advantage in terms of operation is substantial: we move from 192 to 10 quadrature points. The main feature of this compression procedure is that it always results in the minimum number of points that interpolate a specific polynomial [36]. Indeed, in this case we are considering a quadrature rule of degree 2 so the compression procedure selects 10 quadrature points and properly modifies their weights.

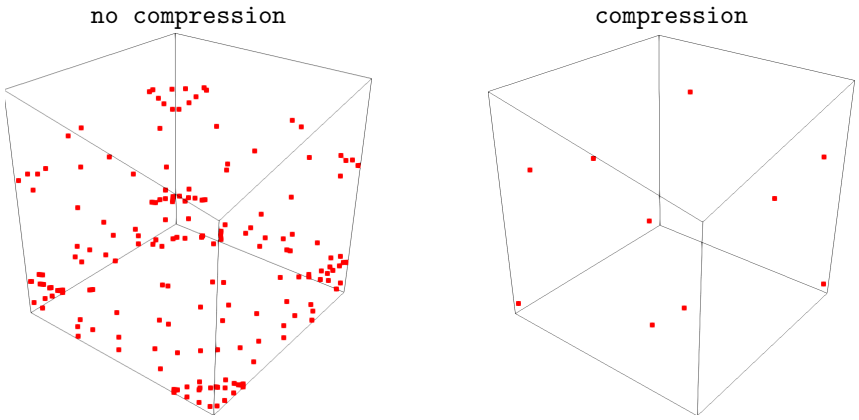


Figure 1: Number of quadrature points without and with the compression procedure. In the former case we have 192 points, while in the latter only 10 points.

**Remark 8.** *To compute $\Psi_3$ it is necessary the quote $\overline{x}_3$. A deeper analysis is required in finding such value, since the quadrature points may fall outside $P$. This is an important issue since the function $\psi$ can be not defined outside $P$. A good idea is to consider not a quote $\overline{x}_3$ but a generic plane that cuts the polyhedron in such a way that all the quadrature points are inside $P$ or at least on the faces of the polyhedron.*

*5.3. Preliminary numerical validation on quadrature weights*

Before dealing with the convergence analysis of Problem (2), we present a numerical example that focuses on the proposed quadrature rule. We consider the following domain

$$\Omega := \{(x_1, x_2, x_3) \in \mathbb{R}^3 \, : \, R_1^2 \leq x_1^2 + x_2^2 \leq R_2^2, \, x_2 \geq 0, \, 0 \leq x_3 \leq 1\} \, ,$$

where $R_1$ and $R_2$ are 0.2 and 1, respectively, and we exploit the proposed quadrature formula, to compute the following integral

$$\int_\Omega \sqrt{x_1^2 + x_2^2} + x_3 \, \mathrm{d}\Omega \, .$$

In Table 1 we compute the relative error varying both the discretizations of $\Omega$ and the quadrature rule degree. More specifically, we are considering two meshes `cyli1` and `cyli2` shown in Figure 2 with descreasing mesh size. From these data we can appreciate that the proposed quadrature rule does converge to the exact value by increasing the polynomial approximation degree and descreasing the mesh size.

| Cylinder example | | |
|---|---|---|
| Gauß degree | `cyli1` | `cyli2` |
| 1 | 1.1263e-03 | 2.5196e-04 |
| 2 | 3.7429e-06 | 2.6066e-06 |
| 3 | 6.0654e-08 | 2.9604e-08 |

Table 1

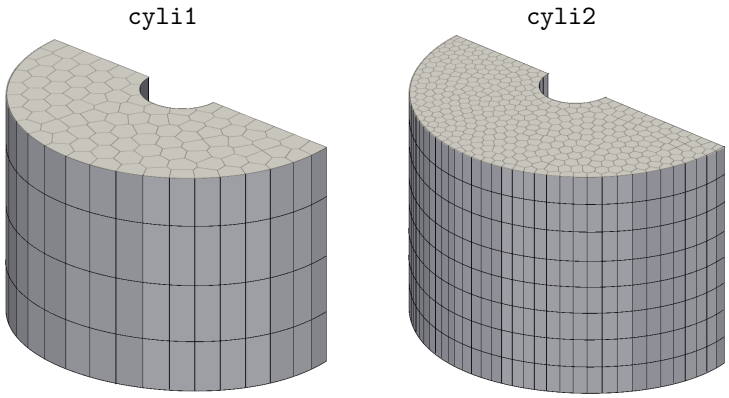


Figure 2: Meshes used to produce the data in Table 1.

## 6. Numerical Examples

In this section we give numerical evidence about the comparison between the straight (`noGeo`) and curved (`withGeo`) approaches, the former being the standard virtual approximation where curved faces are rectified while the latter the one proposed in this work. We consider different kinds of meshes and describe how we build them inside each subsection. Regardless of the type of tessellation we associate to each mesh the mesh-size

$$h = \frac{1}{N_P} \sum_{P \in \Omega_h} h_P \,,$$

where $N_P$ is the number of polyhedrons in $\Omega_h$.

To proceed with the convergence analysis of the errors, we build a sequence of meshes with decreasing $h$ and we compute the following errors indicators:

- $L^2$-error on the velocity field

$$e^{\boldsymbol{v}}_{L^2} := \sqrt{\sum_{P \in \Omega_h} \|\boldsymbol{\Pi}^0_k \boldsymbol{v}_h - \boldsymbol{v}\|^2_0} \,,$$

  where $\boldsymbol{\Pi}^0_k \boldsymbol{v}_h$ is the element-wise $L^2$-projection operator of the virtual element variable $\boldsymbol{v}_h$ inside the polyhedron $P$ and $\boldsymbol{v}$ is the known exact vector field;

- $L^2$-error on the pressure

$$e^{p}_{L^2} := \|p_h - p\|_{0,\Omega} \,,$$

  where $p_h$ is the element-wise polynomial that represents the pressure and $p$ is the exact pressure distribution.

From the theoretical point of view the error $e^{\boldsymbol{v}}_{L^2}$ has a decay of $O\left(h^{k+1}\right)$ while the decay of $e^{p}_{L^2}$ is $O\left(h^{k}\right)$. However, when we consider $k = 2, 3$ and the `noGeo` case, we get $O\left(h^{2}\right)$, whereas only the novel `withGeo` approach will give the expected trend for each $k$.

Such behavior is justified by the following remark. Let us suppose that the error in a numerical scheme can be split in two parts

$$\texttt{err} = \texttt{errApp} + \texttt{errGeo} \,. \tag{40}$$

On the one hand, we make an error in approximating the functional continuous spaces with a discrete one. Such error is related to degree of the polynomial used inside the discrete space taken into account, `errApp`. On the other hand, we make an error in approximating the computational domain $\Omega$ with a mesh $\Omega_h$, `errGeo`.

When we consider standard domains, i.e., domains whose boundaries are planes, elements with straight faces perfectly match such boundaries so `errGeo`

is null. Consequently the error of (40) consists only on the first part and we have

$$\texttt{err} = \texttt{errApp} + 0 = \texttt{errApp} \sim O\left(h^{k+1}\right) , \tag{41}$$

for $e^{\boldsymbol{v}}_{L^2}$ and

$$\texttt{err} = \texttt{errApp} + 0 = \texttt{errApp} \sim O\left(h^{k}\right) , \tag{42}$$

for $e^{p}_{L^2}$, respectively. As a consequence we get the expected convergence rates since the geometrical error disappears.

However, when we are dealing with domains whose boundaries are curved, if we approximate them via elements with straight faces, the geometrical error is not null. It is related only to the mesh size and not on the approximation of the functional spaces we are using. More specifically, if we consider straight faces, it is always $O\left(h^2\right)$. Consequently, for PDEs defined over curve domains (40), it becomes

$$\texttt{err} = \texttt{errApp} + \texttt{errGeo} \sim O\left(h^{k+1}\right) + O\left(h^2\right) = O\left(h^{\min\{k+1,2\}}\right) ,$$

for $e^{\boldsymbol{v}}_{L^2}$ and

$$\texttt{err} = \texttt{errApp} + \texttt{errGeo} \sim O\left(h^{k}\right) + O\left(h^2\right) = O\left(h^{\min\{k,2\}}\right) ,$$

for $e^{p}_{L^2}$, respectively. Thus, when we have a curved boundaries and we consider a mesh with straight faces, the expected rate of $e^{\boldsymbol{v}}_{L^2}$ is achieved only if $k = 1$, otherwise `errGeo` overcomes `errApp`. While $e^{p}_{L^2}$ is achieved if $k = 1$ and 2, and `errGeo` overcomes `errApp` for $k = 3$.

If we use the proposed approach, i.e., we modify the functional spaces in such a way that they can handle elements with curved faces, the geometrical error becomes null. Indeed, since we include the space the map $\gamma$ that exactly describes the geometry, we do not make any error in approximating curved boundaries or interfaces via the functional spaces. Thus, we recover the expected convergence rate as in (41) and (42).

**Remark 9 (Meshes).** *For a boundary face, it is not a priori guaranteed that its vertexes lay on the same plane so we need to sub-triangulate such polygons in order to proceed with the* `noGeo` *approach. Then, if we make such sub-triangulation, the* `noGeo` *and* `withGeo` *case are not comparable in terms of degrees of freedom since the former requires more degrees of freedom with respect to the latter. However, for the domain considered in this work, it is possible to constuct planar quadrilaterals in a starghtforward way so there is no need to subtriangulate faces and* `noGeo` *and* `withGeo` *are comparable in terms of degrees of freedom.*

### *6.1. Example 1: convergence analysis with Dirichlet boundary*

We consider a domain composed by five planar faces and one curvilinear face defined by

$$\Gamma = \left\{ (x_1,\, x_2,\, x_3) \in \mathbb{R}^3 \,:\, x_3 + \frac{1}{10}\,\sin(\pi x_1) - 1 = 0 \right\} .$$

We define the right-hand side and the boundary conditions in such a way that the solution of Problem 2 is

$$p(x_1,\, x_2,\, x_3) := \left(x_3 + \frac{1}{10}\,\sin(\pi x_1) - 1\right)^2 \quad \text{and} \quad \boldsymbol{q} = -\nabla p\,,$$

with $\kappa = \mu = 1$ and we impose essential boundary conditions on all the boundaries including the curved one. In Figure 3 we show one of the meshes taken into account to collect the error for the convergence analysis of the errors $e^{\boldsymbol{v}}_{L^2}$ and $e^{p}_{L^2}$.

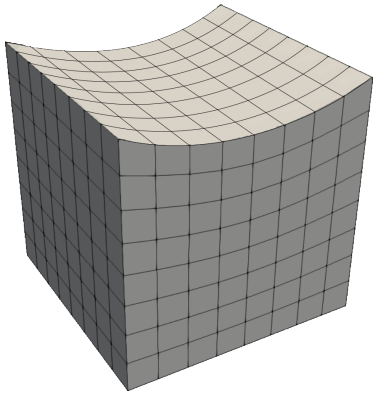

Figure 3: Example 1: one of the mesh taken into account for the convergence analysis for the `withGeo` case.

In Figure 4 we show the convergence plots for such errors varying the VEM approximation degrees for both the `noGeo` and `withGeo` case. More specifically, dashed and full lines represent the error obtained via the `noGeo` and `withGeo` approach, respectively.

As it was already discussed at the beginning of this section, for $k = 1$ these two numerical schemes behave as expected, i.e., $e^{\boldsymbol{v}}_{L^2}$ has an error trend of $O(h^2)$ while $e^{p}_{L^2}$ has $O(h^1)$. However, if we consider $k = 2$ and 3 the trends of `noGeo` and `withGeo` are different. Indeed, $e^{\boldsymbol{v}}_{L^2}$ behaves as $O(h^2)$ for all $k$ in the `noGeo` strategy, while we see the expected convergence rate in the `withGeo` approach. For the $e^{p}_{L^2}$ the behavior of `noGeo` and `withGeo` are different for $k = 3$ since only in this case the geometrical error overcomes the error due to the functional spaces used.

Moreover, by comparing such convergence lines of $e^{\boldsymbol{v}}_{L^2}$ we have the numerical evidence about what we have inferred at the beginning of this section. Indeed, the lines of the error for the `noGeo` case coincides varying the degree $k > 1$, i.e., `errGeo` is too large and such convergence lines are actually `errGeo` for each degree $k$.

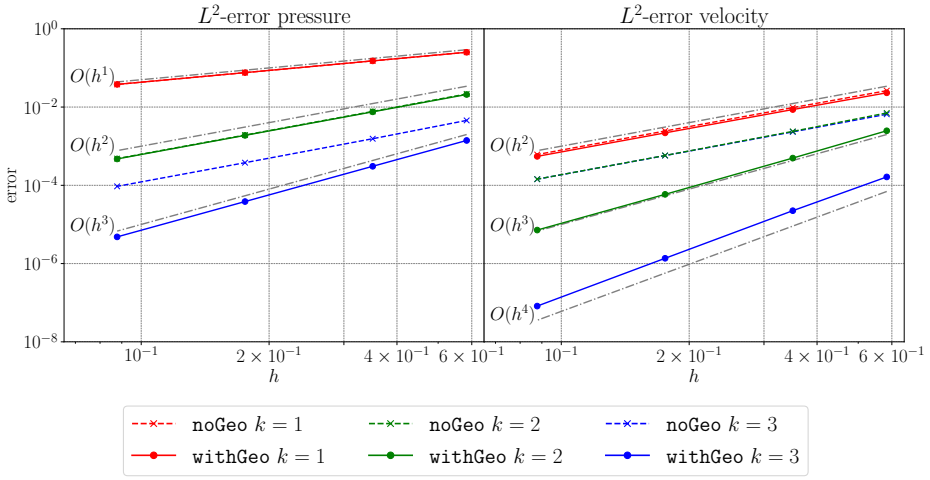


Figure 4: Example 1: convergence lines for both $e^{\boldsymbol{v}}_{L^2}$ and $e^{p}_{L^2}$.

### *6.2. Example 2: convergence analysis with Neumann boundary*

In this section we consider as computational domain

$$\Omega := \{(x_1, x_2, x_3) \in \mathbb{R}^3 \ : \ R_1^2 \leq x_1^2 + x_2^2 \leq R_2^2,\, x_2 \geq 0,\, 0 \leq x_3 \leq 1\}\,,$$

where $R_1$ and $R_2$ are 0.2 and 1, respectively. On such domain we consider Problem 2 where the exact solution is

$$p(x_1, x_2, x_3) = \sin(\pi x_1)\,\cos(\pi x_2)\,\sin(\pi x_3) \quad \text{and} \quad \boldsymbol{q} = -\nabla p\,.$$

and on planar boundaries we impose essential boundary conditions, while on the inner and outer curved boundary we impose natural boundary conditions.

To get a computational domain of such geometry, we extrude along the $z$ axis a two-dimensional polygonal mesh, see Figure 5. We consider two types of two dimensional meshes to extrude: a mesh composed by squares and one composed by triangles. We refer to such meshes as `quad` and `tria`, respectively.

In Figure 6 we collect the convergence lines for each type of mesh. As already seen in the previous example we got the expected error trend for all degrees with `withGeo` approach. The `noGeo` has the expected trend for $k = 1$ in both error indicators, for $k = 2$ it has the expected only for $e^{p}_{L^2}$ and it is $O(h^2)$ for both error indicators when we consider an approximation degree $k = 3$.

### *6.3. Example 3: corner point meshes*

We consider now a particular kind of curved cells: the corner point elements. Such cells have the topology of a cube but their top and bottom faces are bilinear surfaces, i.e., they are defined by the following map $\gamma : [0,\, 1]^2 \to \mathbb{R}^3$

$$\gamma(u,\, v) = (1-u)(1-v)\boldsymbol{x}_A + u(1-v)\boldsymbol{x}_B + (1-u)v\,\boldsymbol{x}_C + u\,v\,\boldsymbol{x}_D\,,$$

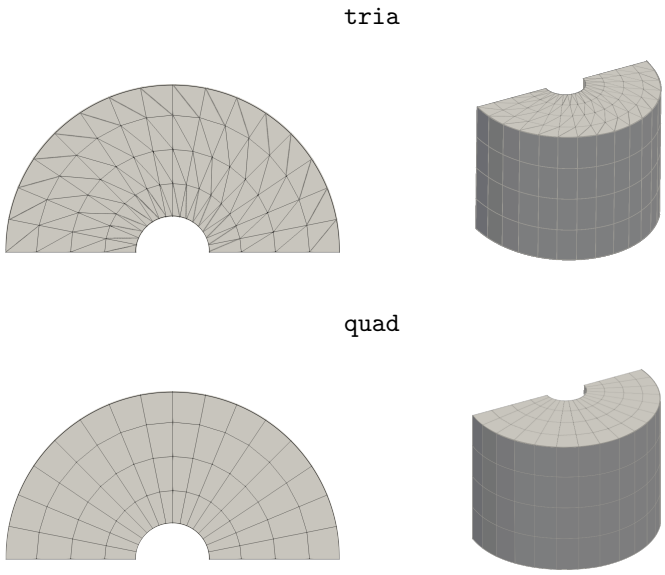


Figure 5: Example 2: on the left the two-dimensional meshes we are extruding, on the right the final meshes. In both cases we are showing the `withGeo` meshes.

where $\boldsymbol{x}_A$, $\boldsymbol{x}_B$, $\boldsymbol{x}_C$, and $\boldsymbol{x}_D$ are the 4 points at the top (or at the bottom) of the cell. In oil industry basins and reservoirs are usually described by this type of meshes [3].

We solve Problem 2 in a unit cube $\Omega = [0, 1]^3$ composed of three layers of materials characterized by different values of permeability. More specifically, the top and the bottom layers have $\kappa = 1$. while the middle one has $\kappa = 0.01$. We set natural boundary conditions on the top and bottom faces of the domain, i.e., the pressure variable is equal to zero at the top and equals to one at the bottom. Then, we consider the force term equal to zero. We consider only a VEM approximation degree $k = 2$ as a representative degree, similar consideration can be done for $k > 2$.

Since we do not have the exact solution, we can not compute the error and we will give only a qualitative analysis on the pressure we get. Moreover, we consider three refinement levels of the mesh at hand to ensure that the method does converge to plausible solution. We refer to such refinement levels as `ref 1`, `2` and `3`, see Figure 7.

We further underline that in such discretizations all the mesh elements are corner point cells so the proposed virtual element incorporates the curved geometry within the function space definition. Thanks to this approach we do not need to introduce any approximation of the curved faces. Moreover, we do not need to sub-triangulate them and introduce further degrees of freedom and, consequently, increase the size of the linear system at hand.

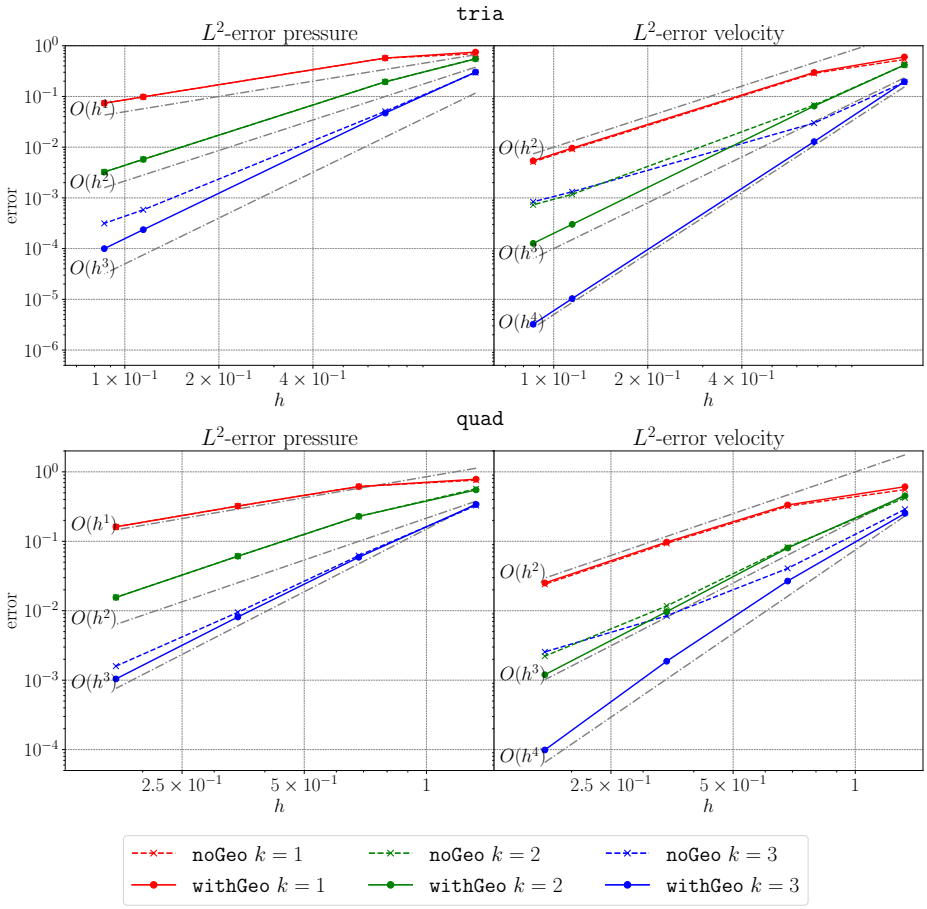


Figure 6: Example 2: convergence lines for both $e^{\boldsymbol{v}}_{L^2}$ and $e^{p}_{L^2}$.

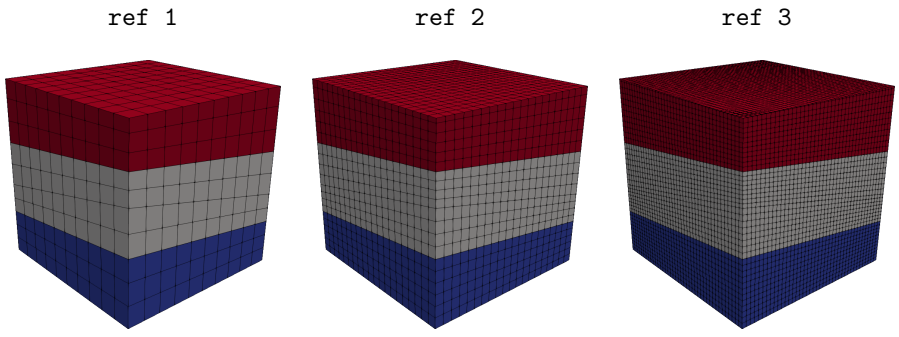


Figure 7: Example 3: refinement levels of the mesh with different layers.

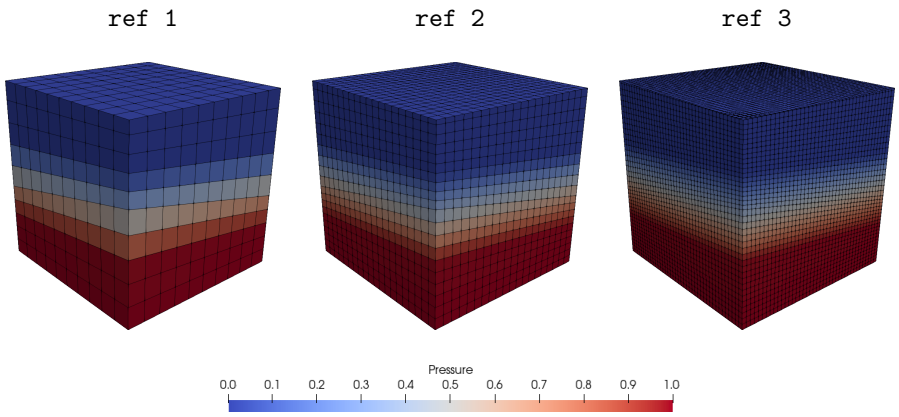


Figure 8: Example 3: pressure filed with three different refinement levels.

From the solutions in Figure 8, we observe a steep change of the pressure values. This fact is expected since we are considering different values of the permeability $\kappa$. Furthermore, such change of pressure is better captured by mesh refinement.

## 7. Conclusions

In this work, we have proposed a mixed virtual element scheme in three space dimensions to solve Darcy problems. The considered scheme handles curved portions of boundary or internal interfaces without any degradation of the expected order of convergence rate. Moreover, since the proposed functional spaces coincide with the ones used for the standard case if the element has no curved faces, it can be seen as a natural extension of the standard case. We also proposed a theoretical analysis to show how to define the approximation spaces and degrees of freedom and we made an analysis on the interpolation properties of the propsed numerical scheme.

Such method also required the definition a suitable quadrature rule to deal with polyhedrons characterized by curved faces. In this paper we propose a possible strategy which still need a deep theoretical analysis. However, such idea is validated by an ad-hoc numerical experiment and implicitly proven by the subsequent convergence analysis on the Darcy problems.

Finally, several numerical tests further show that the proposed scheme achieves the expected order without any degradation due to geometrical errors. Moreover, the last applicative example underlines that the proposed approach can be applied to real life applications characterized by the presence of corner point cells avoiding sub-tetrahedrization that may increase the computational effort.

**Acknowledgments**

This paper is the last checkpoint of the project "Bend VEM 3d". All authors acknowledge INdAM-GNCS which made possible this interesting and long journey.

**References**

[1] J. Bear, C.-F. Tsang, G. de Marsily, Flow and contaminant transport in fractured rock, Academic Press, San Diego, 1993.

[2] C. W. MacMinn, M. L. Szulczewski, R. Juanes, $CO_2$ migration in saline aquifers. Part 1. Capillary trapping under slope and groundwater flow, Journal of Fluid Mechanics 662 (2010) 329–351. doi:10.1017/S0022112010003319.

[3] J. E. Aarnes, S. Krogstad, K.-A. Lie, Multiscale mixed/mimetic methods on corner-point grids, Computational Geosciences 12 (3) (2008) 297–315. doi:10.1007/s10596-007-9072-8.

[4] L. Beirão da Veiga, F. Brezzi, A. Cangiani, G. Manzini, L. D. Marini, A. Russo, Basic Principles of Virtual Element Methods, Mathematical Models and Methods in Applied Sciences 23 (01) (2013) 199–214. doi:10.1142/S0218202512500492.

[5] L. Beirão da Veiga, F. Brezzi, L. D. Marini, A. Russo, The Hitchhiker's Guide to the Virtual Element Method, Mathematical Models and Methods in Applied Sciences 24 (08) (2014) 1541–1573. doi:10.1142/S021820251440003X.

[6] F. Brezzi, R. S. Falk, D. L. Marini, Basic principles of mixed Virtual Element Methods, ESAIM: Mathematical Modelling and Numerical Analysis 48 (4) (2014) 1227–1240. doi:10.1051/m2an/2013138.

[7] L. Beirão da Veiga, F. Dassi, A. Russo, High-order Virtual Element Method on polyhedral meshes, Computers & Mathematics with Applications 74 (5) (2017) 1110–1122. doi:10.1016/j.camwa.2017.03.021.

[8] L. Beirão da Veiga, F. Brezzi, F. Dassi, L. D. Marini, A. Russo, A Family of Three-Dimensional Virtual Elements with Applications to Magnetostatics, SIAM Journal on Numerical Analysis 56 (5) (2018) 2940–2962. doi:10.1137/18M1169886.

[9] L. Beirão da Veiga, F. Dassi, G. Vacca, The Stokes complex for Virtual Elements in three dimensions, Mathematical Models and Methods in Applied Sciences 30 (03) (2020) 477–512. doi:10.1142/S0218202520500128.

[10] M. Frittelli, A. Madzvamuse, I. Sgura, Bulk-surface virtual element method for systems of PDEs in two-space dimensions, Numer. Mat. 147 (2) (2021) 305–348. doi:10.1007/s00211-020-01167-3.

[11] F. Bassi, L. Botti, A. Colombo, D. Di Pietro, P. Tesini, On the flexibility of agglomeration based physical space discontinuous Galerkin discretizations, J. Comput. Phys. 231 (1) (2012) 45–65. doi:10.1016/j.jcp.2011.08.018.

[12] T. Warburton, A low-storage curvilinear discontinuous Galerkin method for wave problems, SIAM J. Sci. Comput. 35 (4) (2013) A1987–A2012. doi:10.1137/120899662.

[13] J. J. Chan, , R. Hewett, T. Warburton, Weight-adjusted discontinuous Galerkin methods: curvilinear meshes, SIAM J. Sci. Comput. 39 (6) (2017) A2395–A2421. doi:10.1137/16M1089198.

[14] E. L. Kawecki, Finite element theory on curved domains with applications to discontinuous Galerkin finite element methods, Numer. Methods Partial Differential Equations 36 (2020) 1492–1536. doi:10.1002/num.22489.

[15] L. Botti, D. Di Pietro, Assessment of Hybrid High-Order methods on curved meshes and comparison with discontinuous Galerkin methods, J. Comput. Phys. 370 (2018) 58–84. doi:10.1016/j.jcp.2018.05.017.

[16] L. Beirão da Veiga, A. Russo, G. Vacca, The Virtual Element Method with curved edges, ESAIM: Mathematical Modelling and Numerical Analysis 53 (2) (2019) 375–404. doi:10.1051/m2an/2018052.

[17] F. Dassi, A. Fumagalli, D. Losapio, S. Scialò, A. Scotti, G. Vacca, The Mixed Virtual Element Method on curved edges in two dimensions, Computer Methods in Applied Mechanics and Engineering 386 (2021) Article Number 114098. doi:10.1016/j.cma.2021.114098.

[18] F. Dassi, A. Fumagalli, I. Mazzieri, A. Scotti, G. Vacca, A Virtual Element Method for the wave equation on curved edges in two dimensions, Journal of Scientific Computing 90 (1) (2022) Article Number 50. doi:10.1007/s10915-021-01683-w.

[19] L. Beirão da Veiga, F. Brezzi, L. D. Marini, A. Russo, Polynomial preserving virtual elements with curved edges, Mathematical Models and Methods in Applied Sciences 30 (08) (2020) 1555–1590. doi:10.1142/S0218202520500311.

[20] P.-A. Raviart, J.-M. Thomas, A mixed finite element method for second order elliptic problems, Lecture Notes in Mathematics 606 (1977) 292–315. doi:10.1007/BFb0064470.

[21] F. Brezzi, J. Douglas, D. L. Marini, Two families of mixed finite elements for second order elliptic problems, Numerische Mathematik 47 (2) (1985) 217–235. doi:10.1007/BF01389710.

[22] F. Brezzi, J. Douglas, R. Durán, M. Fortin, Mixed finite elements for second order elliptic problems in three variables, Numerische Mathematik 51 (2) (1987) 237–250. doi:10.1007/BF01396752.

[23] J. E. Roberts, J.-M. Thomas, Mixed and hybrid methods, in: Handbook of numerical analysis, Vol. II, Handb. Numer. Anal., II, North-Holland, Amsterdam, 1991, pp. 523–639. doi:10.1016/S1570-8659(05)80041-9.

[24] D. Boffi, F. Brezzi, M. Fortin, Mixed Finite Element Methods and Applications, Springer Series in Computational Mathematics, Springer Berlin Heidelberg, 2013. doi:10.1007/978-3-642-36519-5.

[25] L. Beirão da Veiga, F. Brezzi, L. D. Marini, A. Russo, H(div) and H(curl)-conforming VEM, Numerische Mathematik 133 (2) (2014) 303–332. doi:10.1007/s00211-015-0746-1.

[26] L. Beirão da Veiga, F. Brezzi, L. D. Marini, A. Russo, Mixed virtual element methods for general second order elliptic problems on polygonal meshes, ESAIM: Mathematical Modelling and Numerical Analysis 50 (3) (2016) 727–747. doi:10.1051/m2an/2015067.

[27] A. Fumagalli, E. Keilegavlen, Dual Virtual Element Method for Discrete Fractures Networks, SIAM Journal on Scientific Computing 40 (1) (2018) B228–B258. doi:10.1137/16M1098231.

[28] M. F. Benedetto, A. Borio, S. Scialò, Mixed Virtual Elements for discrete fracture network simulations, Finite Elements in Analysis and Design 134 (2017) 55–67. doi:10.1016/j.finel.2017.05.011.

[29] A. Fumagalli, E. Keilegavlen, Dual Virtual Element Methods for Discrete Fracture Matrix Models, Oil & Gas Science and Technology - Revue d'IFP Energies nouvelles 74 (41) (2019) 1–17. doi:10.2516/ogst/2019008.

[30] M. F. Benedetto, S. Berrone, S. Pieraccini, S. Scialò, The virtual element method for discrete fracture network simulations, Computer Methods in Applied Mechanics and Engineering 280 (2014) 135–156. doi:http://dx.doi.org/10.1016/j.cma.2014.07.016.

[31] M. F. Benedetto, S. Berrone, A. Borio, S. Pieraccini, S. Scialò, A hybrid mortar virtual element method for discrete fracture network simulations, Journal of Computational Physics 306 (2016) 148 – 166. doi:10.1016/j.jcp.2015.11.034.

[32] L. Beirão da Veiga, A. Pichler, G. Vacca, A virtual element method for the miscible displacement of incompressible fluids in porous media, Computer Methods in Applied Mechanics and Engineering 375 (2021) Article Number 113649. doi:10.1016/j.cma.2020.113649.

[33] O. Čertík, F. Gardini, G. Manzini, L. Mascotto, G. Vacca, The p-and hp-versions of the virtual element method for elliptic eigenvalue problems, Computers & Mathematics with Applications 79 (7) (2020) 2035–2056.

[34] G. N. Gatica, S. Meddahi, On the coupling of vem and bem in two and three dimensions, SIAM Journal on Numerical Analysis 57 (6) (2019) 2493–2518.

[35] A. Sommariva, M. Vianello, Gauss-green cubature and moment computation over arbitrary geometries, Journal of Computational and Applied Mathematics 231 (2) (2009) 886–896. doi:10.1016/j.cam.2009.05.014.

[36] A. Sommariva, M. Vianello, Compression of Multivariate Discrete Measures and Applications, Numerical Functional Analysis and Optimization 36 (9) (2015) 1198–1223. doi:10.1080/01630563.2015.1062394.

[37] R. A. Adams, Sobolev spaces, Vol. 65 of Pure and Applied Mathematics, Academic Press, New York-London, 1975.

[38] S. C. Brenner, L. R. Scott, The Mathematical Theory of Finite Element Methods, 3rd Edition, Vol. 15 of Texts in Applied Mathematics, Springer, New York, 2008. doi:10.1007/978-0-387-75934-0.

[39] V. Girault, P.-A. Raviart, Finite Element Methods for Navier-Stokes Equations, Vol. 5 of Springer Series in Computational Mathematics, Springer-Verlag Berlin Heidelberg, 1986. doi:10.1007/978-3-642-61623-5.

[40] C. Bernardi, Optimal Finite-Element Interpolation on Curved Domains, SIAM Journal on Numerical Analysis 26 (5) (1989) 1212–1240. doi:10.1137/0726068.